Energy dependence of fusion evaporation-residue cross sections in the ^{28}Si$+^{28}$Si reaction

M. F. Vineyard, J. S. Bauer, C. H. Gosdin, and R. S. Trotter
Department of Physics, University of Richmond, Richmond, Virginia 23173

D. G. Kovar, C. Beck,* D. J. Henderson, R. V. F. Janssens, B. D. Wilkins,[†]
G. Rosner,[‡] P. Chowdhury,[§] H. Ikezoe,[**] and W. Kuhn[††]
Physics Division, Argonne National Laboratory, Argonne, Illinois 60439

J. J. Kolata and J. D. Hinnefeld[‡‡]
Department of Physics, University of Notre Dame, Notre Dame, Indiana 46556

C. F. Maguire
Department of Physics and Astronomy, Vanderbilt University, Nashville, Tennessee 37235

J. F. Mateja
Division of Educational Programs, Argonne National Laboratory, Argonne, Illinois 60439

F. W. Prosser
Department of Physics, University of Kansas, Lawrence, Kansas 66045

G. S. F. Stephans
Laboratory for Nuclear Science, Massachusetts Institute of Technology, Cambridge, Massachusetts 02139
(Received 29 September 1989)

Velocity distributions of mass-identified evaporation residues produced in the ^{28}Si$+^{28}$Si reaction have been measured at bombarding energies of 174, 215, 240, 309, 397, and 452 MeV using time-of-flight techniques. These distributions were used to identify evaporation residues and to separate the complete-fusion and incomplete-fusion components. Angular distributions and total cross sections were extracted at all six bombarding energies. The complete-fusion evaporation-residue cross sections and the deduced critical angular momenta are compared with lower energy data and the predictions of existing models.

I. INTRODUCTION

The large kinetic energies and angular momenta that heavy ions bring into a reaction allow nuclei to be studied under extreme conditions of excitation energy and deformation. An experimental determination of the fusion cross section behavior and an understanding of the limiting processes at high energy can provide information on the effects of angular momentum and excitation energy on the stability of the compound nucleus and the relationship between the cross section for fusion and other reaction channels. Progress in obtaining this understanding has been hampered, however, by the presence of incomplete-fusion (ICF) processes, whose cross sections become significant at bombarding energies above 10 MeV/nucleon.[1-4] The evaporation residues (ER's) from ICF are difficult to distinguish experimentally from those arising from complete fusion (CF). Also, at high energies the ER yields must be distinguished from the products of binary reactions that can populate some of the same mass groups.

In this paper the results of fusion ER cross section measurements for ^{28}Si$+^{28}$Si at bombarding energies of 174, 215, 240, 309, 397, and 452 MeV are presented. The motivation for this study was to further investigate two recent observations. The first is that the ICF process appears to depend on the mass asymmetry in the entrance channel.[5] The second is that a comparison of the complete-fusion evaporation-residue (CFER) cross sections for different systems forming the ^{56}Ni compound nucleus at high excitation energy show that the cross sections for the symmetric entrance-channel reactions are larger than expected.[6]

The experimental procedure is described in Sec. II. In Sec. III the data analysis is discussed and the experimental results are presented. The results are discussed in the context of previous measurements and existing models in Sec. IV and a summary is presented in Sec. V.

II. EXPERIMENTAL PROCEDURE

The experiments were performed using pulsed ^{28}Si beams obtained from the Argonne National Laboratory ATLAS facility. In the measurements at bombarding energies of 174, 215, and 240 MeV the beams were incident on a self-supporting (125 μg/cm^2), isotopically enriched (99.9%), ^{28}Si target mounted at the entrance of a 165 cm scattering chamber. A time-of-flight (TOF) telescope was

M. F. VINEYARD *et al.*

mounted on a variable length arm, pivoted at the target so as to provide a flight path longer than 100 cm at all angles studied. The telescope consisted of three detectors: a gridless, carbon foil (20 μg/cm^2) microchannel plate (MCP) detector 31 cm from the target, a second MCP detector near the end of the arm, and a 250-μm Si surface barrier detector mounted immediately behind the second MCP. Time-of-flight measurements between the first and second MCP's, and between the first MCP and the Si detector were made and used with the energy measurement of the Si detector to establish mass identification.

In the measurements at 309, 397, and 452 MeV the beam was incident on a self-supporting (200 μg/cm^2) ^{28}Si target mounted in the ATLAS 91 cm scattering chamber. Mass identification of the reaction products was obtained with the use of two TOF detectors. The first TOF arm consisted of a MCP detector to provide the start signal and a $\Delta E - E$ Si telescope to obtain the stop signal (ΔE) and full energy ($\Delta E + E$) of each particle. The length of the flight path was 89.8 cm and the resolution of the time measurement was approximately 120 ps full width at half maximum (FWHM). In the second TOF arm, a $\Delta E - E$ Si telescope was again used to obtain the stop (ΔE) and full energy ($\Delta E + E$) signals. However, mass identification was achieved using the rf beam timing of ATLAS. The length of the flight path was 65.6 cm and the time resolution of the ^{28}Si beam pulses was better than 150 ps. An example of the mass resolution attained is shown in Fig. 1. The ER's were stopped in the ΔE detectors at all three energies and the E detectors were used to measure the elastic scattering.

In both sets of measurements the beam direction was established to within 0.05° from left and right measurements of the elastic scattering of ^{28}Si from a ^{197}Au target at small angles (3°–5°). In the measurements at the three higher energies the relative angle between the two TOF arms and the solid angles of the detectors were established from elastic scattering of tandem energy ^{28}Si (76.5 MeV) and ^{58}Ni (79 MeV) beams from the ^{197}Au target. Both the Faraday cup beam integrator and a monitor detector were used to establish the relative normalization between different runs. The two normalizations were found to be in agreement. Absolute cross sections were determined by measuring the elastic scattering of 76.5 MeV ^{28}Si ions from the ^{28}Si target at $\theta_{lab} = 5°$–30° and comparing with the Mott scattering predictions. The cross sections have been corrected for the efficiencies of the MCP detectors.

The energy and time calibrations of the detectors were obtained from the elastic scattering of ^{28}Si ions from the ^{197}Au target, along with the 5.486 MeV alpha group from an ^{241}Am source. In the set of measurements performed at higher bombarding energies, a ^{58}Ni beam was also used. Each measured fragment energy was corrected event by event for energy losses in the target, channel plate foil, gold layers on the fronts of the Si detectors, and aluminum layer on the back of the ΔE detector when applicable. Pulse-height defect corrections based upon the method of Kaufman *et al.*[7] were made for each of the Si detectors. The scaling factor of the pulse-height defect
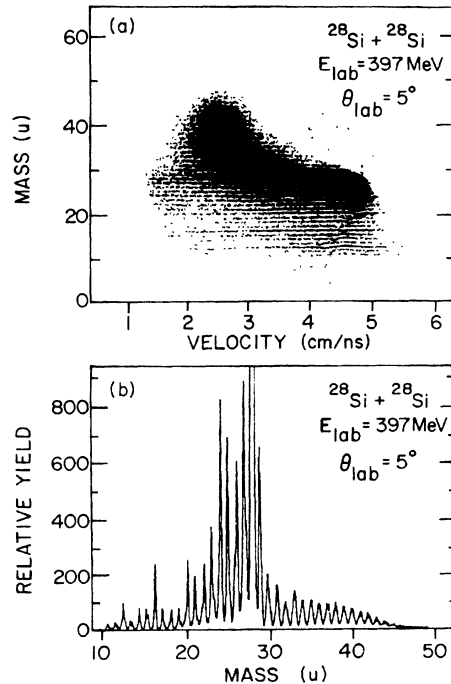
FIG. 1. (a) Two-dimensional mass versus velocity spectrum for ^{28}Si + ^{28}Si at $E_{lab} = 397$ MeV and $\theta_{lab} = 5°$. (b) The corresponding mass spectrum. A software gate on the energy was used to exclude the elastic scattering from these spectra.

correction was determined for each Si detector from the pulse heights induced by the elastically scattered tandem energy ^{28}Si and ^{58}Ni ions. Plasma decay corrections that affect the timing signal obtained from Si detectors were also applied to the data following the prescription of Bohne *et al.*[8]

The velocities of the reaction products measured at 174, 215, and 240 MeV were obtained from the MCP-MCP TOF measurements. Those obtained at the three higher bombarding energies were extracted using two complimentary techniques: (1) by direct TOF measurement corrected for plasma delay, and (2) using the measured energies corrected for pulse-height defect and energy losses along with the mass identification. Good agreement between the two sets of velocity spectra was found. The uncertainty in the velocity measurement of the ER's is estimated to be $+/-0.025$ cm/ns.

III. DATA ANALYSIS AND EXPERIMENTAL RESULTS

The velocity spectra of the reaction products were used to distinguish between ER yields and those arising from other processes like deep inelastic and fusion fission. They were also used to extract information about the relative contributions of CF and ICF. In this section we discuss how the ER yields were identified and how they were decomposed into CF and ICF contributions.

The difficulty in extracting the ER yields can be understood upon an inspection of Fig. 1. Shown in this figure is a two-dimensional mass versus velocity spectrum and a

one-dimensional mass spectrum taken at a bombarding energy of 397 MeV and a laboratory angle of 5°. It is obvious that at this energy there is not a distinct separation between ER's and products from other reaction processes as is the case at lower bombarding energy. For lower ER masses there is clear evidence of a reaction component that does not follow the average velocity of the center of mass. This can be seen in Fig. 2, where the Galilean-invariant velocity spectra $[(1/v^2)d^2\sigma/d\Omega\,dv]$ for masses 40 and 30 are shown. The velocity distribution for $A=40$ is Gaussian and typical of what is observed for the heavier masses. The velocity spectrum for $A=30$, on the other hand, shows evidence of additional components.

To extract ER yields, the Galilean-invariant cross sections for the ER's are assumed to have a Gaussian shaped distribution, with a possible broader width than expected for CF due to the contribution from ICF. This assumption is based on the behavior observed for the heavier ER masses, where there is little ambiguity in the identification, and on the results of calculations with the statistical-model code PACE.[9] In studies involving asymmetric systems, the magnitude of the shift of the velocity centroid with respect to that expected for CF is understood to reflect the relative importance of ICF contributions. The shift is generally expressed in terms of the ratio

$$R_v = V_{centroid}/(V_{c.m.}\cos\theta_{lab}) \ ,$$

where $V_{c.m.}$ is the center-of-mass velocity of the system and θ_{lab} is the laboratory angle at which the centroid is observed. The velocity $V_{c.m.}\cos\theta_{lab}$ is the average velocity expected for ER's produced in a CF reaction assuming the evaporated light particles are emitted isotropically in
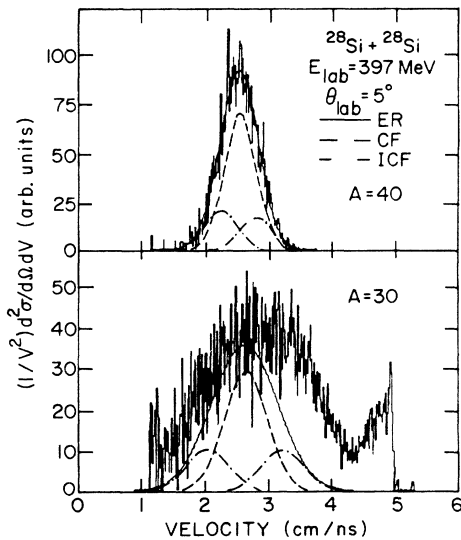
the frame of the compound nucleus.[10] It has recently been shown[6] that anisotropic emission of the evaporated particles produces small deviations from the simple $V_{c.m.}\cos\theta_{lab}$ behavior, but the shapes for all practical purposes remain Gaussian. For symmetric systems, one would expect the presence of ICF contributions to appear as a broadening of the velocity distributions rather than a shift in the centroid. This is in fact exactly what is observed in the present measurements at the three highest energies as illustrated in Figs. 3 and 4. The ratios R_v extracted from the 397 MeV data are shown in Fig. 3 plotted as a function of (a) mass at $\theta_{lab}=5°$ and (b) angle for mass 38. The solid horizontal lines are the results expected assuming isotropic emission of the evaporated light particles and the dashed curves are the results of a PACE calculation. The data are in good agreement with the predictions. The widths (FWHM) of the velocity distributions at $E_{lab}=397$ MeV, plotted as a function of (a) mass at $\theta_{lab}=5°$ and (b) angle for mass 38, are shown in Fig. 4. The PACE calculation (solid curve) correctly predicts the trend of the mass and angle dependence of the widths. However, the magnitude of the widths is underpredicted indicating the presence of ICF processes. This discrepancy between the observed and predicted widths was found at the three highest bombarding energies, increasing with the bombarding energy. At the three lower bombarding energies studied the widths observed were in basic agreement with the PACE predictions, indicative of small or no ICF contributions.

The invariant ER cross sections for each mass were extracted for the reactions at the three lower bombarding

FIG. 2. The Galilean-invariant velocity spectra observed for masses 40 and 30 at $E_{lab}=397$ MeV and $\theta_{lab}=5°$. The curves are the Gaussian fits to the data as described in the text. The sharp cutoff at high velocity in the $A=30$ spectrum is the result of a software gate on the energy to exclude the elastic scattering.
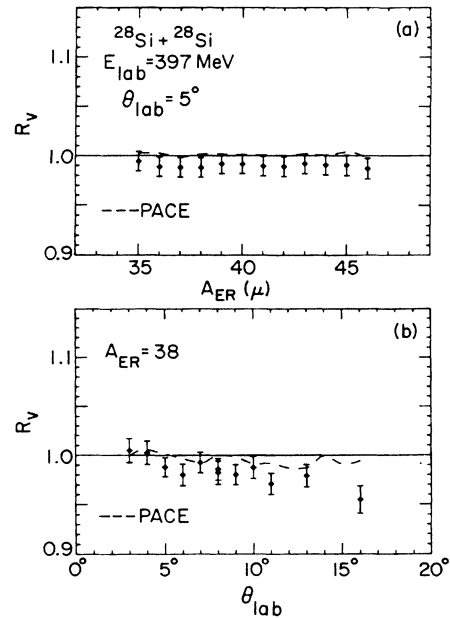
FIG. 3. The ratios $R_v = V_{centroid}/(V_{c.m.}\cos\theta_{lab})$ extracted from the 397 MeV data plotted as a function of (a) mass at $\theta_{lab}=5°$ and (b) angle for mass 38. The solid horizontal lines indicate the results expected assuming isotropic emission of the evaporated light particles and the dashed curves are the results of PACE calculations.
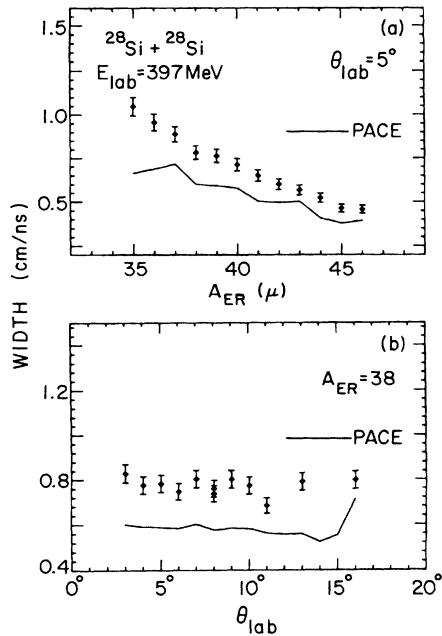
FIG. 4. The widths (FWHM) of the velocity distributions at $E_{\text{lab}} = 397$ MeV plotted as a function of (a) mass at $\theta_{\text{lab}} = 5°$ and (b) angle for mass 38. The solid lines represent the predictions of the code PACE.

energies by identification of yields associated with the observed Gaussian shaped velocity distributions. At these energies the procedure was straightforward with little ambiguity except for the lighter ER masses at back angles, where contributions to the cross section were small. The invariant ER cross sections for the reactions at the three higher bombarding energies were determined for each mass using a Gaussian shaped velocity distribution with the centroid predicted by PACE and a width allowed to vary smoothly with mass. The mass dependence of the width was established by fitting the heavier masses. For the heavier masses, such as $A = 40$ at $E_{\text{lab}} = 397$ and $\theta_{\text{lab}} = 5°$, whose velocity spectrum is shown in Fig. 2, this procedure was straightforward and yields were obtained with relatively small uncertainties. For the lighter masses, larger uncertainties are associated with this procedure. Because of the presence of deep inelastic and fission components in the velocity spectra of these lighter masses, it is sometimes difficult to identify a Gaussian component and, even when a Gaussian component is apparent, it is difficult to estimate the "background" contributions. In these cases, the yields were extracted by adjusting the amplitude of the Gaussian to the maximum value consistent with the data. An example of this is shown in Fig. 2 for $A = 30$ at $E_{\text{lab}} = 397$ MeV and $\theta_{\text{lab}} = 5°$. These yields are considered to be maximum limits on the ER yields. It was not clear from the data how far down to lower masses this procedure should be carried. Therefore, we chose to include those masses that together correspond to 99% of the PACE predicted mass distribution. Statistical model calculations for ICF processes yield mass distributions that are only slightly shift-

ed to lower masses indicating that this is a reasonable procedure. The angle-integrated ER mass distributions for the three highest energies are shown in Fig. 5. In Fig. 6 are shown the angular distributions of the total ER cross sections extracted at the six bombarding energies studied.

Once the ER yields were identified they were decomposed into CF and ICF contributions. For the three lower bombarding energies the predicted widths of the velocity distributions are similar enough to those observed that no attempt was made to decompose the distributions. At the three higher energies the decomposition was accomplished by fitting the ER component of the velocity spectrum for each mass with the sum of three Gaussians as shown in Fig. 2 for $A = 40$ and 30 at $E_{\text{lab}} = 397$ MeV and $\theta_{\text{lab}} = 5°$. The middle Gaussian is assumed to be the CF component, while the outer two Gaussians represent the ICF contributions. In the fitting procedure, the centroid of the middle Gaussian and the widths of all three were fixed, while the amplitude of all three and the position of the outer two were varied to fit the data. The values for the centroid and width of the CF Gaussian were taken from the PACE predictions. The widths of the ICF components were assumed to be equal to that of the CF component. The further constraint that the position of the outer Gaussians be symmetric about the position of the middle Gaussian was also applied. Statistical-model calculations for ICF processes in which it is assumed that a preequilibrium α particle escapes from either the projectile or the target indicate that these assumptions are reasonable. The angle-integrated CF mass distributions are compared to those of the ER's and
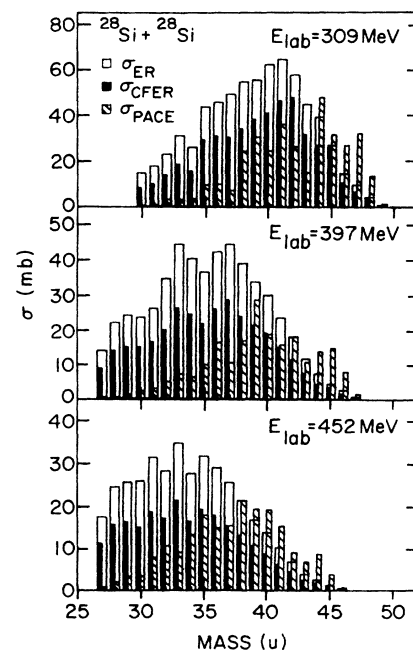
FIG. 5. Angle-integrated evaporation-residue (ER) and complete-fusion evaporation-residue (CFER) mass distributions compared with the PACE predictions.
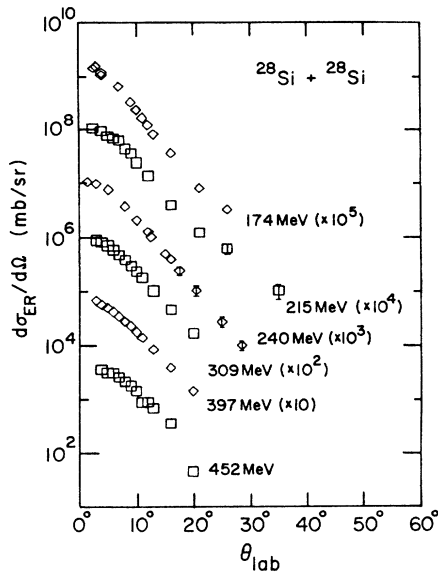
FIG. 6. Angular distributions of the total evaporation-residue cross sections extracted at the six bombarding energies studied.

the PACE predictions in Fig. 5. The summed angular distributions for the ER yields (squares) and the CF yields (diamonds) obtained using the procedures described earlier are presented in Fig. 7.

The total ER cross sections and the total CFER cross sections, found by integrating the angular distributions
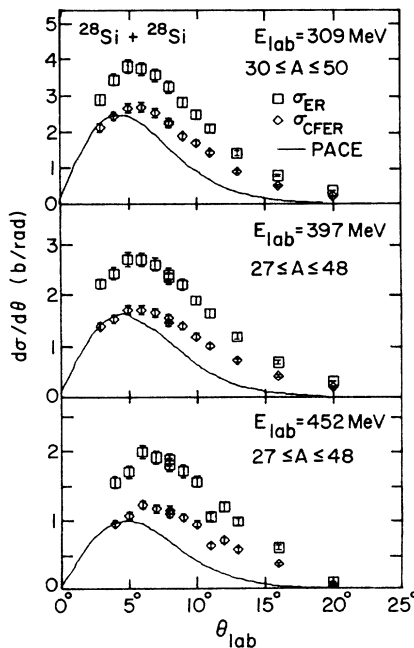
FIG. 7. The total evaporation-residue (squares) and complete-fusion (diamonds) angular distributions resulting from the decomposition of the velocity spectra at the three higher energies. The solid curves are PACE predictions normalized to the most forward angle data points.

TABLE I. Experimental cross sections.

$E_{\rm lab}$ (MeV)	$\sigma_{\rm ER}$ (mb)	$\sigma_{\rm CFER}$ (mb)
174	852+/−85	852+/−85
215	788+/−78	788+/−78
240	708+/−70	708+/−70
309	685+/−103	470+/−94
397	525+/−79	326+/−65
452	372+/−56	229+/−46

(using a smooth extrapolation at the two angular extremes), are listed in Table I. The cross sections listed for the three higher bombarding energies must be considered to be upper limits. The uncertainty in the absolute ER cross sections at the three lower energies arise from counting statistics, uncertainties in the absolute normalization, and extrapolations out of the measured angular ranges. In addition to these, the errors given for the ER cross sections at the three higher energies include uncertainties in the procedure used to extract the yields for the lighter masses. The errors associated with the CF cross sections at the higher energies also include uncertainties due to the fitting procedure.

IV. DISCUSSION

The solid curves in Fig. 7 are the CFER angular distributions predicted by PACE and normalized to the data at forward angles. As can be seen, the measured angular distributions are broader and peak at a larger angle than the predictions. In an attempt to understand the origin of this discrepancy, the angular distributions of the individual mass residues were studied. It was found that the heavy residue masses were fairly well predicted by the PACE calculations over the entire angular range. However, discrepancies between the experimental and predicted angular distributions begin to appear for the lighter residue masses and become more evident as the residue mass decreases. This is illustrated in Fig. 8, where the extracted and calculated CFER angular distributions for $A=45$, 40, and 35 at $E_{\rm lab}=397$ MeV are compared. A disagreement between the data and the predictions of CF evaporation calculations also exists in the mass distributions as shown in Fig. 5. The PACE predicted mass distribution is shifted to larger mass with respect to the extracted CF mass distribution. These observations are consistent with those of a very recent study[6] of $^{16}{\rm O}+^{40}{\rm Ca}$ at $E_{\rm lab}(^{16}{\rm O})=214$ MeV. There it was suggested that these discrepancies between the experiment and predictions are due to the inability of the evaporation codes to include the emission of heavy particles. Heavy particle evaporation could certainly produce a broadening in the angular distributions of the lighter ER's and a shift in the mass distributions. However, experimental verification will have to await coincidence measurements. It should be noted that the possibility cannot be ruled out that the effects observed here may be due at least in part to misidentification of the yields at larger angles for the lighter masses.

The total CFER cross sections measured in the present study are plotted along with previous lower-energy mea-
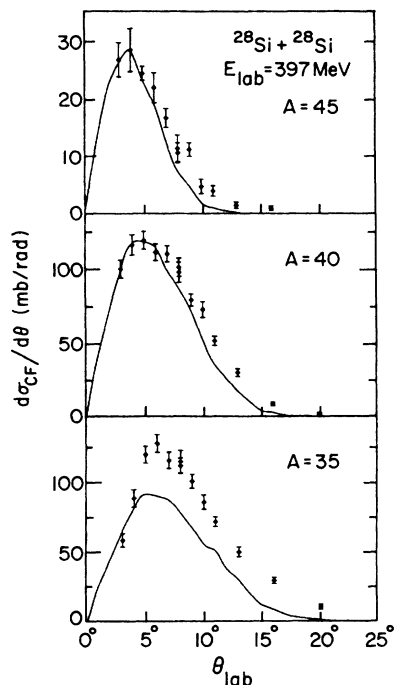
FIG. 8. Complete-fusion evaporation-residue angular distributions measured for $A = 45, 40$, and 35 at $E_{lab} = 397$ MeV. The solid curves are the results of a PACE calculation normalized to the most forward angle data points.

surements[11,12] in Fig. 9. The solid, dashed, and dot-dashed curves shown in the figure are the predictions at the critical distance,[13] the surface friction,[14] and the proximity[15] fusion models, respectively. The experimental cross sections in the high-energy region are overpredicted by all three of these entrance-channel models. This discrepancy may reflect the fact that fission channels are implicitly included in the model calculations, but not in the data. The total fission cross section behavior for
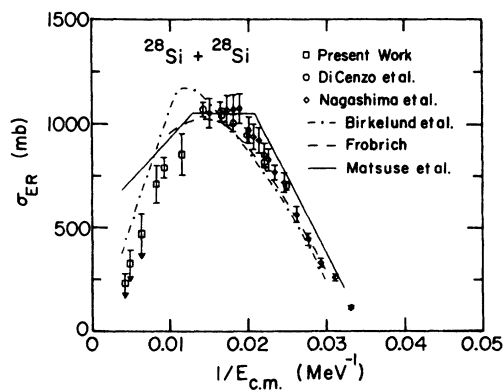
FIG. 9. Complete-fusion evaporation-residue cross sections for the ^{28}Si + ^{28}Si reaction. The data points are from Ref. 11 (circles), Ref. 12 (diamonds), and the present work (squares). The solid, dashed, and dot-dashed curves represent the results of fusion-model calculations of Refs. 13, 14, and 15, respectively.

^{28}Si + ^{28}Si has not been established. However, recent studies of ^{16}O + ^{40}Ca (Refs. 6 and 16) and ^{32}S + ^{24}Mg (Ref. 17), which form the same compound nucleus, have indicated the presence of a substantial fission cross section. In light of these results, one might expect a significant fission cross section for ^{28}Si + ^{28}Si at these energies. Coincidence measurements are needed to determine if the fission cross sections could indeed account for this discrepancy. Another possible explanation for the overprediction of the high-energy cross sections by the entrance-channel models is that the ICF process may compete with CF for the same partial waves. Therefore these models, which assume that all partial waves that reach some critical distance of approach lead to CF, would overestimate the CF cross section at high bombarding energy. Fusion cross sections for the ^{28}Si + ^{28}Si system have also been calculated by Bonche *et al.*[18] and Hong *et al.*[19] in the framework of the time-dependent Hartree-Fock (TDHF) approximation. However, the falloff of the cross section at high energy in these calculations corresponds to the occurrence of a low-l window in the fusion partial cross sections that has never been verified experimentally.

For purposes of comparison, the CFER cross sections for ^{28}Si + ^{28}Si (Refs. 11 and 12), ^{16}O + ^{40}Ca (Refs. 6, 12, and 20), and ^{32}S + ^{24}Mg (Refs. 21–23) are plotted as a function of $Z_1 Z_2 / E_{c.m.}$ in Fig. 10. It can be seen that all three systems exhibit a very similar energy dependence. This suggests a common limitation on the CFER cross section that might be associated with the properties of the ^{56}Ni compound nucleus.

The critical angular momenta extracted from the experimental ^{28}Si + ^{28}Si, ^{32}S + ^{24}Mg, and ^{16}O + ^{40}Ca CFER cross sections using the sharp cutoff approximation are plotted versus the excitation energy of the ^{56}Ni compound nucleus in Fig. 11. There are three distinct regions of this plot that can be associated with different types of limitations of the CF cross sections. At low excitation energies, the fusion cross section is determined by the ability to penetrate the interaction barrier. In the intermediate excitation energy range $(60 < E^* < 90$ MeV),
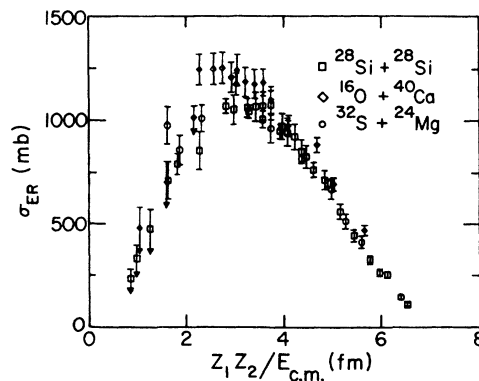
FIG. 10. Complete-fusion evaporation-residue cross sections for the ^{28}Si + ^{28}Si (squares; Refs. 11, 12, and present work), ^{16}O + ^{40}Ca (diamonds; Refs. 6, 12, and 20), and ^{32}S + ^{24}Mg (circles; Refs. 21–23) are plotted as a function of $Z_1 Z_2 / E_{c.m.}$.
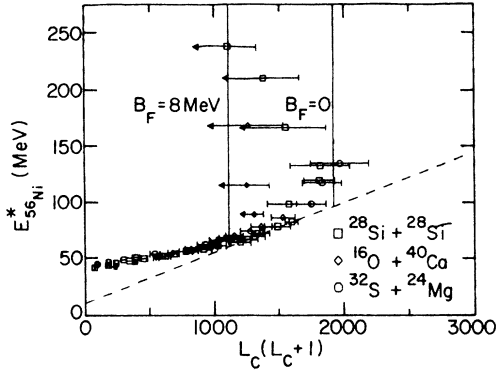
FIG. 11. Compound-nucleus excitation energy versus the product of the critical angular momenta extracted from the complete-fusion cross sections shown in Fig. 10. The dashed line corresponds to a statistical yrast line (Ref. 24) with $\Delta Q = 10$ MeV and $r_0 = 1.20$ fm. The solid vertical lines indicate the predicted angular momenta for fission barriers of $B_F = 0$ and 8 MeV using the model of Sierk (Ref. 27).

the fusion process for the three systems appears to be limited in a common way[24,25] by the properties of the compound nucleus. The dashed line shown in the figure is the statistical yrast line[24] calculated with $r_0 = 1.2$ fm and $\Delta Q = 10$ MeV. The behavior of all three systems in the intermediate excitation energy range is reproduced rather well by this line. At higher excitation energies, more severe limitations on the CF cross sections appear to occur. It has been pointed out in a previous study[26] that both CF and ICF seem to be limited by fission competition. The solid vertical lines in Fig. 11 correspond to the angular momenta at which the calculated fission barrier of ^{56}Ni vanishes ($B_F = 0$ MeV) and at which it is approximately equal to the nucleon separation energy ($B_F = 8$ MeV), where one expects fission to become competitive. These calculations were performed with the code of Sierk.[27] The critical angular momenta deduced in this study for ^{28}Si + ^{28}Si at the three lower energies agree with those extracted for the ^{32}S + ^{24}Mg system.[23] As pointed out earlier,[6] these critical angular momenta are somewhat larger than expected based on the calculated fission-barrier limits. Since the results for the ^{16}O + ^{40}Ca system compare rather well with these fission-barrier limits, it was suggested that further measurements were needed to determine whether the observed differences reflect an entrance-channel dependence or the presence of ICF processes, whose contributions to the ER's have been misidentified in the symmetric systems. In this work for ^{28}Si + ^{28}Si, as in the study of ^{32}S + ^{24}Mg,[23] no clear evidence of significant ICF processes is observed at bombarding energies corresponding to the excitation energy range $90 < E^* < 140$ MeV in the ^{56}Ni compound nucleus. On the other hand, the extracted upper limits for the critical angular momenta deduced here for ^{28}Si + ^{28}Si at $E^* > 150$ MeV agree with the ^{16}O + ^{40}Ca result[6] and are somewhat consistent with the calculated fission-barrier limits. The reason for the difference in the extracted critical angular momenta for symmetric and asymmetric systems in the excitation energy range

$90 < E^* < 140$ MeV remains an open question.

The ratios of CF to total ER cross sections of $1.0(+0.0/-0.14)$, $1.0(+0.0/-0.14)$, $1.0(+0.0/-0.14)$, $0.69(+/-0.18)$, $0.62(+/-0.16)$, and $0.61(+/-0.15)$ were obtained at $E_{lab} = 174$, 215, 240, 309, 397, and 452 MeV, respectively. These appear to be consistent with the systematic behavior observed by Morgenstern et al.[5] This is illustrated in Fig. 12, where the observed trends are shown along with the results of the recent ^{16}O + ^{40}Ca measurements[6] and the present work. A common onset of incomplete fusion for systems with different mass asymmetry in the entrance channel is found only when the data are plotted as a function of the center-of-mass velocity of the lighter reaction partner at contact, i.e.,

$$v_L = [A_H/(A_H + A_L)]v_{rel} ,$$

where A_H and A_L are the masses of the heavier and lighter reaction partner, respectively. The relative velocity, v_{rel}, is defined as

$$v_{rel} = [2(E_{c.m.} - V_C)/\mu]^{1/2} ,$$

where $E_{c.m.}$ and V_C are the center-of-mass kinetic and Coulomb energies, respectively, and μ is the reduced mass. Morgenstern suggested that this behavior may indicate that ICF processes are associated with reactions in which the vector coupling of the Fermi motion of the individual nucleons with the relative motion of the interacting nuclei produce nucleons with sufficient velocity to escape.

The widths of the velocity distributions observed in this study at bombarding energies of 309 and 397 MeV are quite consistent with those reported recently for ^{28}Si + ^{nat}Si at $E_{lab} = 347$ MeV.[28] In that study, an analysis of the first moment of the invariant velocity distributions was performed to obtain a value of the average missing momentum that lies between 2.5% and 3.5%. The number of preequilibrium nucleons responsible for this missing momentum can be estimated[3,6] under the assumption that they are emitted along the beam axis with the veloci-
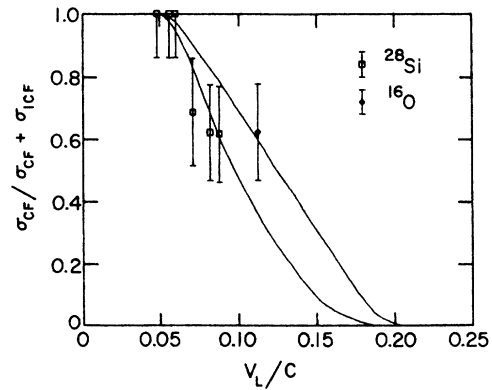
FIG. 12. The ratio of complete-fusion cross section to total evaporation-residue cross section as a function of the velocity of the lighter nucleus V_L/c. The curves represent the trends from Ref. 5 and the data for ^{16}O and ^{28}Si projectiles are from Ref. 6 and the present work, respectively.

ty of the projectile and is found to be approximately 1.5 nucleons. This number should be compared with 2.5 preequilibrium nucleons estimated from the average velocity deficit observed in the $^{16}O + ^{40}Ca$ reaction at $E_{lab}(^{16}O) = 214$ MeV, which is at the same relative velocity at the moment of contact.[6] The comparison supports the systematics of Morgenstern *et al.*,[5] which suggest that ICF is more likely for an asymmetric system than a symmetric system at the same relative velocity. It has been suggested[26] that this is a result of the ICF contribution appearing in the fission channels for the symmetric systems and the ER channel for the asymmetric systems.

V. SUMMARY

Evaporation-residue-like fragments produced in the interaction of ^{28}Si with ^{28}Si at bombarding energies of 174, 215, 240, 309, 397, and 452 MeV have been studied using pulsed beams obtained from the ANL ATLAS facility. Time-of-flight techniques enabled the extraction of the velocity distributions of the resolved ER mass groups. The width of these distributions compared to the predictions of statistical-model calculations indicate the presence of significant ICF processes at the three higher energies. For the three lower energies, there is no clear evidence from the widths of the velocity spectra for ICF contributions. The velocity spectra were used to separate the CF and ICF components with the aid of evaporation-code calculations. Complete angular distributions for ER's were obtained at all six energies and for yields consistent with CF at the three higher energies.

The CF angular distributions at the three higher energies are broader and peak at a larger angle than evaporation-code predictions. Also, the predicted mass distributions are shifted to higher mass than the experimental distributions. Similar observations have been made in an early study and are interpreted as evidence for the presence of heavy particle evaporation or very mass-asymmetric fission.

The total CFER cross sections extracted at the three lower bombarding energies agree with those measured previously for the $^{32}S + ^{24}Mg$ system in the compound nucleus excitation energy range $90 < E^* < 140$ MeV. These cross sections are somewhat larger than those reported recently for the $^{16}O + ^{40}Ca$ system in the same excitation energy range. They are also larger than expected based on recent fission-barrier calculations. The upper limits of the CFER cross sections at the three higher energies, on the other hand, are consistent with the $^{16}O + ^{40}Ca$ result at compound nucleus excitation energies above 150 MeV. Further measurements are needed to establish the fusion-fission cross section behavior as a function of energy for all three systems in order to better understand the limitations imposed on the CF process.

The ratios of CF to total ER cross sections and the widths of the velocity distributions obtained in this study appear to be consistent with previously established systematics that argue for an entrance-channel mass-asymmetry dependence of the ICF process. However, additional experiments, particularly coincidence measurements, need to be performed to verify this behavior.

ACKNOWLEDGMENTS

*Present address: Centre de Recherches Nucleaires, Strasbourg, France.
†Present address: Energy and Environmental Systems, Argonne National Laboratory, Argonne, IL 60439.
‡Present address: Institut fur Kernphysik der Universitat Mainz, Postf. 3980, D-6500 Mainz, Federal Republic of Germany.
§Present address: Yale University, New Haven, CT 06511.
**Present address: Japan Atomic Energy Research Institute, Tokai Research Establishment, Tokai-Mura, Ibaraki-Ken, Japan.
††Present address: Universitat Giessen, Giessen, West Germany.
‡‡Present address: Kernfysisch Versneller Institute, NL9747AA, Groningen, The Netherlands.
[1] H. Morgenstern, W. Bohne, K. Grabisch, D. G. Kovar, and H. Lehr, Phys. Lett. 113B, 463 (1982); H. Morgenstern, W. Bohne, K. Grabisch, H. Leher, and W. Stoffler, Z. Phys. A 313, 39 (1983).
[2] G. Rosner, J. Pochodzalla, B. Heck, G. Hlawatsch, A. Miczaika, J. H. Rabe, R. Butsch, B. Kolb, and B. Sedelmeyer, Phys. Lett. 150B, 87 (1985).
[3] G. S. F. Stephans, D. G. Kovar, R. V. F. Janssens, G. Rosner, H. Ikezoe, B. Wilkins, D. Henderson, K. T. Lesko, J. J. Kolata, C. K. Gelbke, B. V. Jacak, Z. M. Koenig, G. D. Westfall, A. Szanto De Toledo, E. M. Szanto, and P. L. Gonthier, Phys. Lett. 161B, 60 (1985).
[4] Y. Chan, M. Murphy, R. G. Stokstad, I. Tserruya, S. Wald, and A. Budzanowski, Phys. Rev. C 27, 477 (1983).
[5] H. Morgenstern, W. Bohne, W. Galster, K. Grabisch, and A. Kyanowski, Phys. Rev. Lett. 52, 1104 (1984).
[6] C. Beck, D. G. Kovar, S. J. Sanders, B. D. Wilkins, D. J. Henderson, R. V. F. Janssens, W. C. Ma, M. F. Vineyard, T. F. Wang, C. F. Maguire, F. W. Prosser, and G. Rosner, Phys. Rev. C 39, 2202 (1989).
[7] S. B. Kaufman, E. P. Steinberg, B. D. Wilkins, J. Unik, A. J. Gorski, and M. J. Fluss, Nucl. Instrum. Methods 115, 47 (1974).
[8] W. Bohne, W. Galster, K. Grabisch, and H. Morgenstern, Nucl. Instrum. Methods A240, 145 (1985).
[9] PACE is the modification of the code JULIAN described by A. Gavron, Phys. Rev. C 21, 230 (1980).
[10] J. Gomez del Campo, R. G. Stokstad, J. A. Biggerstaff, R. A. Dayras, A. H. Snell, and P. H. Stelson, Phys. Rev. C 19, 2170

(1979).

[11]S. B. DiCenzo, J. F. Peterson, and R. R. Betts, Phys. Rev. C 23, 2561 (1981).

[12]Y. Nagashima, J. Schimizu, T. Nakagawa, Y. Fukuchi, W. Yokota, K. Furuno, M. Yamanouchi, S. M. Lee, N. X. Dai, T. Mikumo, and T. Motobayashi, Phys. Rev. C 33, 176 (1986).

[13]T. Matsuse, A. Arima, and S. M. Lee, Phys. Rev. C 26, 2338 (1982); S. M. Lee and T. Matsuse, J. Phys. Soc. Jpn. 54, 272 (1985); T. Matsuse and S. M. Lee, in Proceedings of the Tsukuba International Symposium on Heavy Ion Fusion Reactions, Tsukuba, 1984 (unpublished); S. M. Lee, W. Yokota, and T. Matsuse, in Proceedings of the Symposium on The Many Facets of Heavy-Ion Fusion Reactions, Argonne, 1985, edited by W. Henning, D. G. Kovar, S. Landowne, and S. Pieper, Argonne National Laboratory Report No. ANL-PHY-86-1, 1986, p. 63.

[14]P. Frobrich, Phys. Rep. 116, 337 (1984).

[15]J. R. Birkelund, L. E. Tubbs, J. R. Huizenga, J. N. De, and D. Sperber, Phys. Rep. 56, 107 (1979); J. R. Birkelund and J. R. Huizenga, Annu. Rev. Nucl. Part. Sci. 33, 265 (1983).

[16]S. J. Sanders, R. R. Betts, I. Ahmad, K. T. Lesko, S. Saini, B. D. Wilkins, F. Videbaek, and B. K. Dichter, Phys. Rev. C 34, 1746 (1986).

[17]S. J. Sanders, D. G. Kovar, B. B. Back, C. Beck, B. K. Dichter, D. J. Henderson, R. V. F. Janssens, J. G. Keller, S. Kaufman, T. F. Wang, B. D. Wilkins, and F. Videbaek, Phys. Rev. Lett. 59, 2856 (1987).

[18]P. Bonche, K. T. R. Davies, B. Flanders, H. Flocard, B. Grammaticos, S. E. Koonin, S. J. Krieger, and M. S. Weiss,

Phys. Rev. C 20, 641 (1979).

[19]S. W. Hong, Y. J. Lee, B. T. Kim, and D. Cha, Phys. Rev. C 39, 2061 (1989).

[20]S. E. Vidgor, D. G. Kovar, P. Sperr, J. Mahoney, A. Menchaca-Rocha, C. Olmer, and M. S. Zisman, Phys. Rev. C 20, 2147 (1979).

[21]H. H. Gutbrod, W. G. Winn, and M. Blann, Nucl. Phys. A213, 267 (1973).

[22]D. G. Kovar, P. D. Bond, C. Flaum, M. J. Levine, and C. E. Thorn, Bull. Am. Phys. Soc. 22, 66 (1977); D. G. Kovar, Proceedings of the IPCR Symposium on Macroscpoic Features of Heavy Ion Collisions and Preequilibrium Processes, Hakone, Japan, 1977 [IPCR Cyclotron Prog. Rep. Suppl. 6, 18 (1977)].

[23]J. D. Hinnefeld, J. J. Kolata, D. J. Henderson, R. V. F. Janssens, D. G. Kovar, K. T. Lesko, G. Rosner, G. F. S. Stephans, A. M. van den Berg, B. D. Wilkins, F. W. Prosser, S. V. Reinert, and P. L. Gonthier, Phys. Rev. C 36, 989 (1987).

[24]S. M. Lee, T. Matsuse, and A. Arima, Phys. Rev. Lett. 45, 165 (1980).

[25]R. Vandenbosch and A. J. Lazzarini, Phys. Rev. C 23, 1074 (1981).

[26]J. Pochodzalla, R. Butsch, B. Heck, and G. Rosner, Phys. Lett. B 181, 33 (1986).

[27]A. J. Sierk, Phys. Rev. Lett. 55, 582 (1985); Phys. Rev. C 33, 2039 (1986).

[28]P. Decowski, E. A. Bakkum, P. F. Box, K. A. Griffioen, R. Kamermans, and R. J. Meijer, Phys. Rev. C 37, 2495 (1988).